J Solid State Electrochem (2015) 19:3401–3410
DOI 10.1007/s10008-015-2976-7

ORIGINAL PAPER

Electrospun porous carbon nanofibers as lithium ion battery anodes

Yi-Te Peng[1] · **Chieh-Tsung Lo**[1]

Received: 19 February 2015 / Revised: 21 May 2015 / Accepted: 14 July 2015 / Published online: 23 July 2015

Abstract Porous carbon nanofibers were fabricated by electrospinning in a precursor solution containing polyacrylonitrile (PAN), polymethyl methacrylate (PMMA), and *N*,*N*-dimethylformamide. During thermal treatment, PMMA decomposition caused nanofibers to transform from a solid to a porous structure. Removal of PMMA also decreased the fiber diameter and increased the pore volume of the carbon nanofibers, resulting in a substantial increase in specific surface area. We used these web-type fiber films directly without a binder as an anode for lithium ion batteries. The electrochemical performance of these 5:5 PAN/PMMA-derived carbon nanofibers exhibited a discharge capacity of 446 mAh/g under a current density of 150 mA/g, which was approximately two times that of the neat PAN-derived carbon nanofibers. Additionally, the discharge capacity retention of the 5:5 PAN/PMMA-derived carbon nanofibers was nearly the same as that of the neat PAN-derived carbon nanofibers, indicating favorable cycle stability.

Keywords Lithium ion battery · Anode materials · Carbon nanofibers · Electrospinning

Introduction

Owing to the growing demands of portable electronic devices and electric vehicles, the development of efficient and high-capacity storage systems is an urgent task. Rechargeable lithium ion batteries are considered one of the promising energy storage technologies because of their high-energy density and long cycle life. Thus, many studies have focused on exploring novel materials for the cathode, anode, and electrolyte components of the battery. Carbon-based materials have favorable properties, such as low cost, easy obtainability, high Coulombic efficiency, and safety, and are conventionally employed as anode materials for lithium ion batteries. However, to meet the requirements for increasingly demanding electronic devices and to expand to larger scale applications, such as utility grids, new types of carbon-based materials must be developed to improve the electrochemical performance of batteries.

In recent years, carbon-based materials with various nanostructures, including carbon nanotubes [1, 2], graphenes [3–5], and carbon nanofibers [6–9], have been developed to improve the performance of lithium ion batteries. Among these nanomaterials, carbon nanofibers, which possess a straight, continuous, and interconnected structure, can increase the electron-conductive pathway and reduce the distance of lithium ion diffusion, leading to low resistance and high capacity when used as an anode for lithium ion batteries. Additionally, they exhibit excellent mechanical strength and can serve as electrode materials without a binder. Therefore, substantial efforts have been made to prepare carbon nanofibers through various approaches [10–12]. Electrospinning, known for its low cost and simple process, is a fiber preparation technique [13, 14]. Precursor polymer nanofibers, prepared by electrospinning and followed by pyrolysis, transform into carbon nanofibers. Electrospun carbon nanofibers exhibit favorable properties, such as nanometer-sized diameters, high-specific surface areas, and web morphologies, making them highly suitable for an anode material.

Many researchers focused on improving the electrochemical performance of electrospun carbon nanofibers. The idea is

✉ Chieh-Tsung Lo
tsunglo@mail.ncku.edu.tw

[1] Department of Chemical Engineering, National Cheng Kung University, No. 1, University Road, Tainan City 701, Taiwan

to fabricate nanostructured fibers to provide high-specific surface area and an open-pore structure. The high-specific surface area allows carbon nanofibers to easily interact with the electrolyte, resulting in the reduction of the electronic and ionic transport distances. Simultaneously, the presence of pores provides additional space for lithium insertion. Ji and Zhang prepared porous carbon nanofibers by electrospinning in a polymer solution composed of polyacrylonitrile (PAN) and poly(L-lactide) (PLLA) [15]. Subsequent thermal treatment allowed PAN carbonization, but eliminated PLLA, to create pores on the nanofibers. Their porous carbon nanofibers exhibited a specific capacity of 435 mAh/g at a current density of 50 mA/g. Following the similar idea, hollow carbon nanofibers were prepared by electrospinning using a co-axial nozzle in which poly(styrene-co-acrylonitrile) copolymer solution is in the core and PAN solution is in the shell [16]. The hollow carbon nanofibers created from the process provided favorable electrochemical performance and could also serve as a container to prepare composite electrodes containing active materials.

Another strategy to improve the electrochemical performance of carbon nanofibers is to implement active materials in carbon nanofibers [17–25]. These active materials normally have higher theoretical reversible capacity than the theoretical reversible capacity of graphite (372 mAh/g). For example, Wang et al. fabricated carbon–cobalt composite nanofibers by electrospinning [17]. The addition of cobalt particles in the carbon nanofibers increased the interfacial surface area between the fibers and electrolyte. Cobalt particles could also enhance electrical conductivity of the fibers. As a result, their composite fibers exhibited a discharge capacity of over 800 mAh/g at a current density of 100 mA/g. Yu et al. incorporated tin nanoparticles in porous multichannel carbon fibers [18]. These composite fibers exhibited a 30 % capacity loss after the first cycle, but capacity retention remained nearly 100 % after 140 cycles, comparing these to commercial tin electrodes, which show rapid degradation after 20 cycles. The encapsulation of nickel nanoparticles in carbon nanofibers was reported as a potential anode material [19]. Nickel nanoparticles could act as a catalyst for Li_2O decomposition and stabilize solid electrolyte interphase (SEI) layers, leading to the reduction of irreversible capacities. Although the addition of active materials to carbon nanofibers considerably increases the specific capacity of fibers, there is an associated increase in cost. In addition, the volume expansion of active materials during the charge–discharge process causes fractures of the conductive network, resulting in poor cycle stability [26, 27].

In this study, we prepared porous carbon nanofibers via electrospinning in a PAN/polymethyl methacrylate (PMMA) precursor solution. PMMA is immiscible with PAN, so macrophase separation occurs during electrospinning. Subsequent thermal treatment at 800 °C carbonizes PAN, but eliminates PMMA, leaving pores on the fiber surface. We varied the concentration of PMMA in the precursor solution and investigated the effect of added PMMA on fiber morphology and the electrochemical performance of carbon nanofibers. The results of this study indicated that the addition of PMMA to prepare electrospun carbon nanofibers effectively increased the specific surface area and pore volume of the fibers. The porous fiber morphology led to a more favorable discharge capacity when compared to those of the neat PAN-prepared carbon nanofibers. Although numerous papers have demonstrated the superior properties of electrospun carbon nanofibers by adding active materials, not much research is focused on the manipulation of morphology of electrospun carbon nanofibers for the use as anode materials for lithium ion batteries. The results presented in this paper are of considerable technological interest showing porous carbon nanofibers without active materials are promising anode materials for lithium ion batteries.

Experimental section

Materials

PAN and PMMA with a molecular weight of 150,000 and 97,000 g/mol, respectively, were provided by Sigma-Aldrich Co. *N*,*N*-dimethylformamide (DMF, 99.8 %) was purchased from Macron Chemicals. All the materials were used as received without further purification.

Preparation of electrospun carbon nanofibers

The precursor solution for electrospinning was prepared by dissolving various compositions of PAN/PMMA in DMF with a concentration of 12 wt%. The solution was vigorous stirred for 24 h at room temperature. A conventional single-nozzle electrospinning process was carried out at room temperature to create fibers. First, the precursor solution was loaded into a 10-mL glass syringe with a 16-G stainless needle tip. The needle tip was connected to a DC power supply (You-Shang Technical Corporation) to provide a voltage of 15 kV. A piece of aluminum foil, placed vertically at a horizontal distance of 15 cm away from the tip, was used to collect the electrospun fibers. During electrospinning, the polymer solution was extruded from the needle at a flow rate of 0.7 mL/h, controlled by a digital syringe pump (KDS 100, KD Scientific). The electrospun fibers were collected and air dried to allow residual solvent to evaporate prior to thermal treatment. Stabilization was carried out by heating the fibers to 250 °C at a heating rate of 5 °C/min in air. The temperature was maintained at 250 °C for 6 h. Subsequently, the temperature was elevated to 800 °C at a heating rate of 2 °C/min and the fibers were carbonized in nitrogen at 800 °C for 1 h.

Characterization

A JEOL (JSM-6700F) scanning electron microscope and a Hitachi (SU8010) scanning electron microscope, both operated at an accelerating voltage of 10 kV, were used to observe the morphology of the electrospun fibers. Prior to SEM measurement, fibers were sputter-coated with a thin layer of platinum using a JEOL JFC-1600 coater to enhance image capture. The average fiber diameter was statistically determined from SEM micrographs by analyzing a population of at least 100 fibers per sample. The nitrogen sorption isotherms were measured at 77 K (ASAP-2020, Micromeritics). Prior to measurement, the carbon nanofibers were degassed at 200 °C under vacuum to remove other adsorbed species. The specific surface area and pore size distribution of carbon nanofibers were evaluated using the Brunauer–Emmett–Teller (BET) and Barrett–Joyner–Halenda (BJH) methods, respectively. The microstructure of carbon nanofibers was determined by a Rigaku RINT-2000 diffractometer with a source of filtered CuKα radiation. The measurement was performed at 40 kV and 40 mA with the diffraction angle (2θ) between 5° and 70° at a scan rate of 4°/min. Raman spectroscopy was conducted on the carbon nanofibers using a DXR Raman microscope (Thermo Fisher Scientific) with a laser excitation wavelength of 532 nm at 0.5 mW.

For the electrochemical studies, the electrospun carbon nanofiber mats were used directly as a binder-free working electrode. Coin cells (type 2032, Ubiq Technology Co., Ltd) were assembled inside an Argon-filled glove box. Lithium metals (99.9 %, Hongda Energy) served as both counter and reference electrodes. The electrolyte used was 1 M $LiPF_6$ dissolved in a mixture of ethylene carbonate/diethyl carbonate/dimethyl carbonate (1:1:1 by volume). A PP-PE-PP trilayer (Celgard M824, 12 μm) was used as the separator. Galvanostatic charge–discharge tests were performed between cutoff potentials of 0.01 and 2.80 V versus Li/Li^+ at a constant current density using a battery test system (BAT750B, Acutech Systems Co., Ltd.). Current densities were varied between 150 and 900 mA/g. The cycling stability tests were evaluated with 100 cycles at a current density of 200 mA/g.

Results and discussion

Morphology and microstructure of electrospun carbon nanofibers

Figure 1 shows the SEM images of electrospun PAN and PAN/PMMA fibers. The as-spun fibers exhibited uniformly cylindrical fibers and randomly arranged morphology without the appearance of beads. The fiber diameter decreased from 1068±123 nm for the neat PAN fibers to 626±101 and 581±139 nm for 7:3 (weight ratio) PAN/PMMA- and 5:5 (weight ratio) PAN/PMMA-derived fibers, respectively. The variation of fiber diameters was caused by the change in precursor

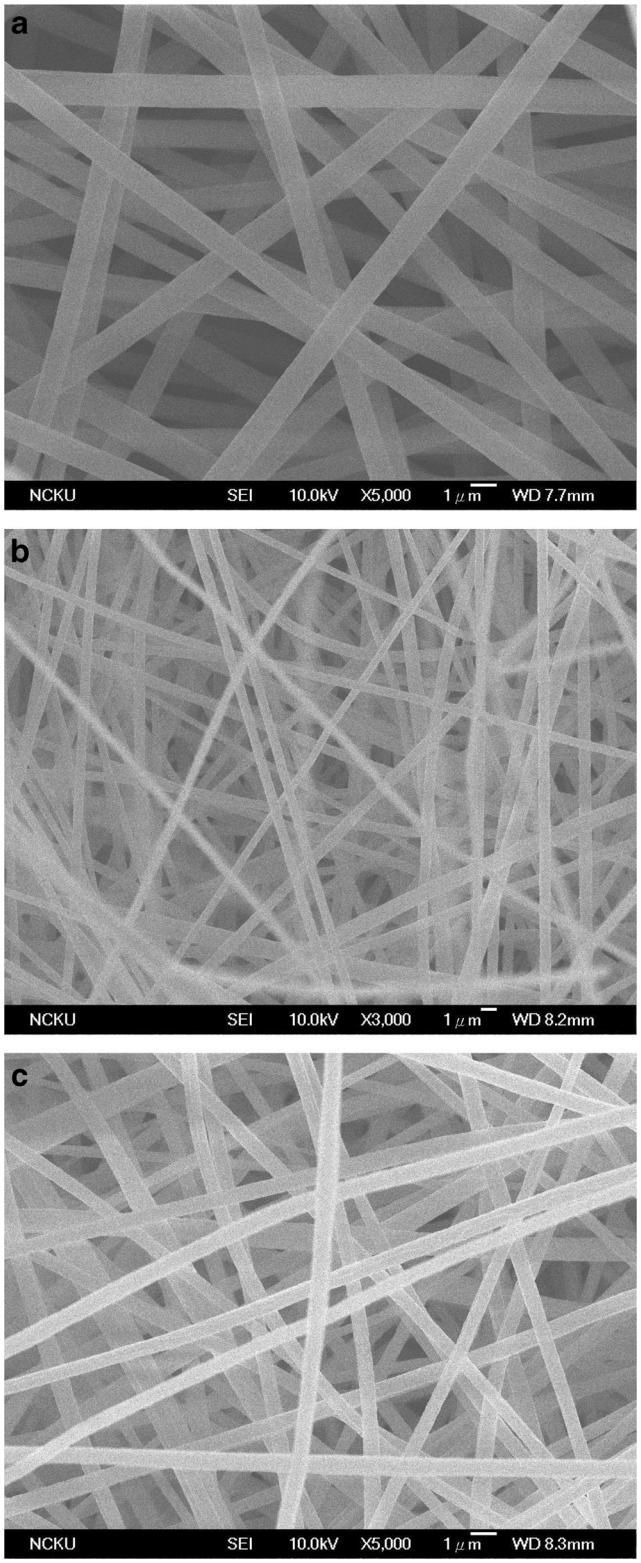

Fig. 1 SEM micrographs of electrospun polymer fibers. **a** PAN/PMMA=10:0; **b** PAN/PMMA=7:3; and **c** PAN/PMMA=5:5

viscosity when the PMMA was added, which altered the spinning conditions.

Figure 2 shows the morphology of the electrospun fibers after carbonization. During stabilization and carbonization, PAN underwent several reactions, including cyclization, dehydration, and crosslinking [28]. Cyclization induced the conversion of nitrile groups (C≡N) to double bond groups (C=N), leading to a thermally stable cyclized structure. The oxidative stabilization step created crosslinks between PAN molecules [29]. Both processes inhibited weight loss and retained the fiber morphology for the subsequent thermal treatment. By contrast, PMMA is unable to form a thermally stable cyclized structure. Instead, it decomposed and was removed during pyrolysis. In Fig. 2a, the carbon nanofibers prepared using neat PAN exhibited long and bead-free morphology. By contrast, the PAN/PMMA-derived carbon nanofibers were uneven and interconnected, particularly for 5:5 PAN/PMMA-derived carbon nanofibers (Fig. 2c, e). The interconnected structure was attributed to the presence of PMMA. PMMA is a thermally liable polymer, which melts during pyrolysis. The PMMA melting softens fibers, which enables neighboring fibers to attach with each other, resulting in fiber to fiber connection. The addition of a thermally liable polymer in PAN to develop an interconnected fiber structure was also reported in several other works [30, 31]. After carbonization, the fiber diameter decreased to 684±53, 401±58, and 344±64 nm for neat PAN-, 7:3 PAN/PMMA-, and 5:5 PAN/PMMA-derived carbon nanofibers, respectively. The shrinkage of all carbon nanofibers was mainly caused by the release of gases, such as CO_2, CO, NH_3, and H_2O. The removal of PMMA also contributed to reduced fiber diameter for the PAN/PMMA-derived carbon nanofibers. Figure 2 also provides the inner structure of the nanofibers. As observed in Fig. 2b, neat

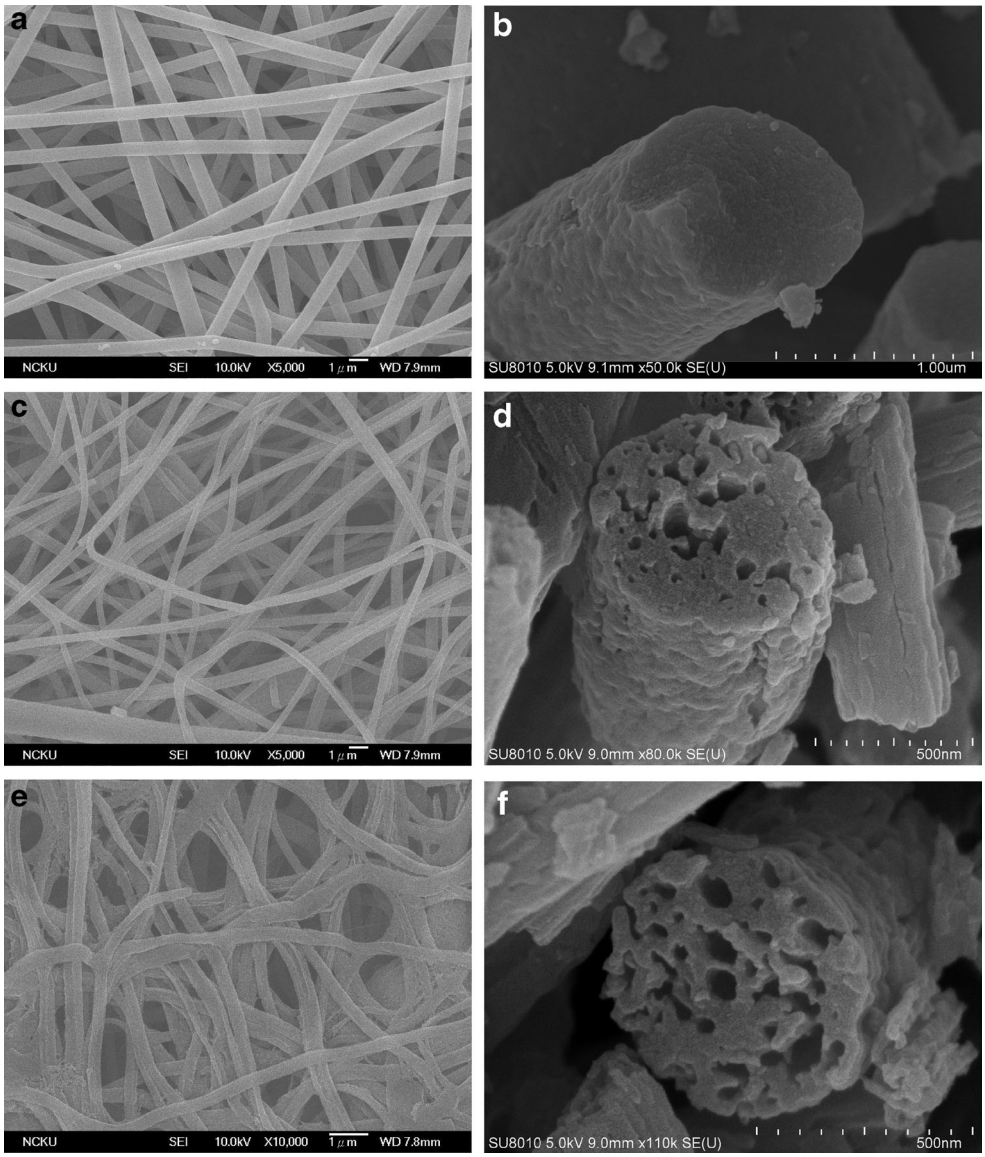

Fig. 2 SEM micrographs of electrospun fibers carbonized at 800 °C. **a** and **b** PAN/PMMA=10:0; **c** and **d** PAN/PMMA=7:3; and **e** and **f** PAN/PMMA=5:5

PAN-derived carbon nanofibers were internally nonporous. The introduction of PMMA in precursor solution facilitated the development of pores and channels inside the carbon nanofibers (Fig. 2d, f). The inner structure of the carbon nanofibers was associated to the phase behavior of PAN/PMMA blends. PAN and PMMA are immiscible and they phase separate [32]. In addition, because the surface tension of PAN (36 dyn/cm) is smaller than that of PMMA (42 dyn/cm) [33, 34], PAN forms the shell and PMMA forms the core of the nanofibers. During thermal treatment, the PMMA was burned off, resulting in the pores and channels inside fibers.

We performed N_2 adsorption isotherms on the electrospun carbon nanofibers to understand the morphological features. As shown in Fig. 3, the adsorption occurring at relative pressure smaller than 0.2 was contributed by micropores. Conversely, the adsorption occurring at relative pressure larger than 0.8 was caused by mesopores. The specific surface area calculated using the BET method and the porosity parameters analyzed using the BJH approach are summarized in Table 1. Both mesopore volume and micropore volume increased with PMMA content. For the neat PAN-derived carbon nanofibers, the pores were generated during thermal treatment because of the release of gases. The addition of PMMA increased the mesopore volume considerably, suggesting that the removal of PMMA also created pores. Other studies have specified that mesopores enable the diffusion of electrolyte ions into carbonaceous materials [35, 36]. By contrast, micropores are not favorable for rapid ion diffusion since they are not easily wetted by electrolytes. Therefore, preparing carbon nanofibers with a large number of mesopores is crucial to improve the electrochemical performance of carbon nanofibers. Table 1 also shows a substantial increase in the specific surface area of fibers when PMMA is added. This is understandable because PAN/PMMA-derived carbon nanofibers exhibited smaller fiber diameter and larger pore volume than the neat PAN-derived carbon nanofibers did. When used as anode materials for lithium ion batteries, carbon nanofibers with a large surface area are accessible to electrolytes. This reduces electronic and ionic transport length and facilitates rapid charging and discharging at high current densities.

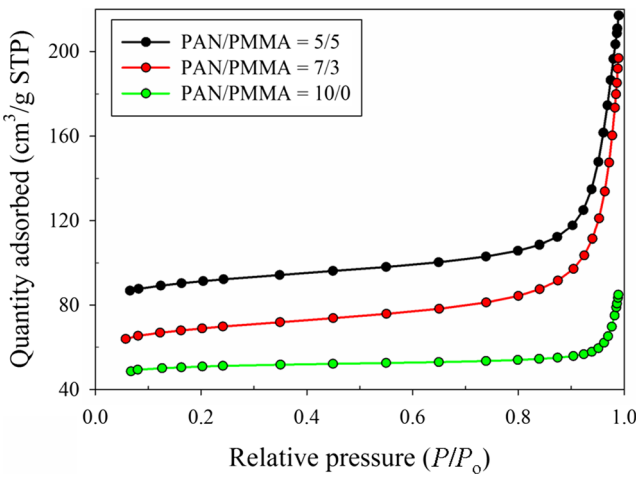

Fig. 3 N_2 adsorption isotherms of electrospun carbon nanofibers

Figure 4 shows the XRD patterns of electrospun carbon nanofibers. The PAN-derived carbon nanofibers exhibited two broad reflections. The strong peak located at 2θ of approximately 25° corresponds to the (002) graphitic layers and the weak peak appeared at 2θ of approximately 45° indicates the (100) turbostratic carbon plane [37]. The addition of PMMA presented similar characteristic patterns without remarkable peak shift. From the XRD patterns, the microcrystallite size of the carbon nanofibers parallel to the edge plane (L_c) was calculated using the Scherrer equation [38].

$$L_c = \frac{k\lambda}{B\cos\theta} \quad (1)$$

where k is the Scherrer constant (which is taken as 0.89 in this work), λ is the wavelength of the incident X-ray beam, and B is the angular width of the peak at a half maximum intensity. The calculated microcrystallite sizes of carbon nanofibers are listed in Table 1. The addition of PMMA caused a slight variation with the microcrystallite size along the c-axis of nanofibers. According to the Bragg equation, the interlayer distance (d_{002}) of the nanofibers was 0.363 nm for all nanofibers regardless of the PMMA amount added. The obtained d_{002} value was larger than the interlayer distance of graphite (0.335 nm), indicating that the microstructure of the electrospun carbon nanofibers is a turbostratic carbon structure with a slightly mismatched layer sequence [39]. The nearly constant values of both L_c and d_{002} were attributed to the immiscibility between PAN and PMMA, causing phase separation and preventing the occurrence of structural rearrangement during pyrolysis.

Crystalline perfection of carbon nanofibers was analyzed using Raman spectroscopy with the results shown in Fig. 5. Two major peaks, located at approximately 1350 and 1582 cm^{-1}, were assigned as the disorder (D peak) and graphite (G peak) bands, respectively [40]. The D band is associated with the defect structure, the edge of the carbon planes, or the disorder structure. By contrast, the G band represents the carbon atom sp^2 in-plane structure or the highly ordered plane structure. The intensity ratio of the D and G bands, $R_I = I_D/I_G$, represents the graphitization degree of the carbon nanofibers. A low R_I value indicates a dominant ordered structure in the fibers. As evidenced by Table 1, the R_I value of the neat PAN-derived carbon nanofibers exhibited a relatively large value, suggesting a high disorder in the fibers. When PMMA was added, the R_I value decreased considerably, suggesting that the addition of PMMA facilitated the conversion of disordered carbonaceous components into more ordered graphite crystallites.

Table 1 The structural properties of various carbon nanofibers after pyrolysis

Sample	D (nm)	S_A (m^2/g)	V_t (cm^3/g)	V_{meso} (cm^3/g)	V_{micro} (cm^3/g)	L_c (nm)	d_{002} (nm)	R_I
PAN/PMMA 10:0	684	170	0.127	0.049	0.078	0.862	0.363	1.55
PAN/PMMA 7:3	401	234	0.294	0.205	0.089	0.768	0.363	1.35
PAN/PMMA 5:5	344	306	0.329	0.208	0.121	0.704	0.363	1.38

D fiber diameter; S_A specific surface area; V_t total pore volume; V_{meso} mesopore volume (1.7–300 nm); V_{micro} micropore volume (<1.7 nm), calculated by $V_t - V_{meso}$; L_c stacking size; d_{002} interlayer spacing of crystallite

Electrochemical performance of electrospun carbon nanofibers

The electrospun carbon nanofibers were used directly as anodes for lithium ion batteries. We performed the galvanostatic charge–discharge and cycle life tests to determine the electrochemical performance of the fibers. Figure 6a shows the galvanostatic charge–discharge curves of the various carbon nanofibers in the first discharge and charge cycle at a current density of 150 mA/g. During discharge, lithium ions were inserted into carbon nanofibers, causing a substantial reduction of the cell potential from the open circuit potential to a potential between 0.75 and 1.2 V. The potential reached a plateau, which lasted until the specific capacity reached approximately 200 mAh/g. After the plateau, the potential decreased slowly to a cutoff potential. During charge, the cell potential increased gradually to a cutoff potential without the occurrence of a plateau. The cells exhibited initial discharge specific capacities of approximately 500, 800, and 950 mAh/g for the PAN-, 7:3 PAN/PMMA-, and 5:5 PAN/PMMA-derived carbon nanofibers, respectively. However, the following charge specific capacities were only 250, 420, and 500 mAh/g for the PAN-, 7:3 PAN/PMMA-, and 5:5 PAN/PMMA-derived carbon nanofibers, respectively. The difference between the discharge and charge specific capacities is the irreversible capacity. The irreversible capacity of all the carbon nanofibers was approximately 40–50 % of the initial discharge capacity. The irreversible capacity was attributed to the development of the SEI layer [41] or structural defects that consumed additional lithium ions [42, 43]. The SEI layer occurred because of the decomposition of the electrolyte in carbonaceous materials during the discharge process, preventing further solvent reduction in subsequent discharge processes. The SEI layer was insulated by electrons but did not prevent the diffusion of unsolvated lithium ions. Because the reactions associated with the formation of the SEI layer were irreversible and consumed excess lithium ions, they induced irreversible capacity. As suggested by Kim et al. [44], the reversible intercalation of Li ions occurred only in graphitic sheets. Therefore, a large fraction of the irreversible capacity for the PAN- and PAN/PMMA-derived carbon nanofibers was because of insufficient development of the carbonized microstructure, which is also confirmed by the Raman spectra. When the discharge–charge process was lasted to the 10th cycle as presented in Fig. 6b, we only observe a gradual decrease of the cell potential during discharge without the appearance of a plateau for any of the samples. Additionally, the discharge and charge specific capacities were nearly equal, suggesting that no irreversible reactions occurred. The discharge specific capacity of the neat PAN-derived carbon nanofibers in the 10th cycle was 211 mAh/g. When PMMA was added, the discharge specific capacity increased to 343 and

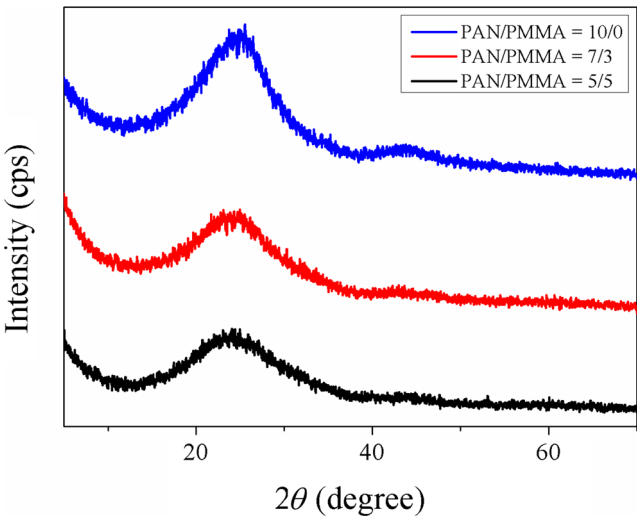

Fig. 4 XRD patterns of electrospun carbon nanofibers

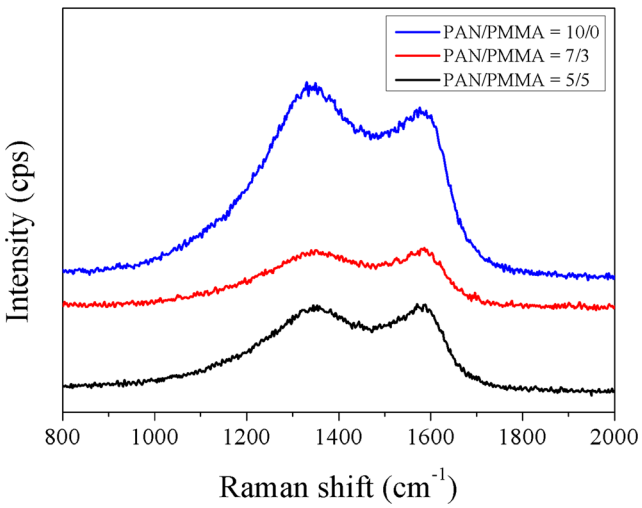

Fig. 5 Raman spectra of electrospun carbon nanofibers

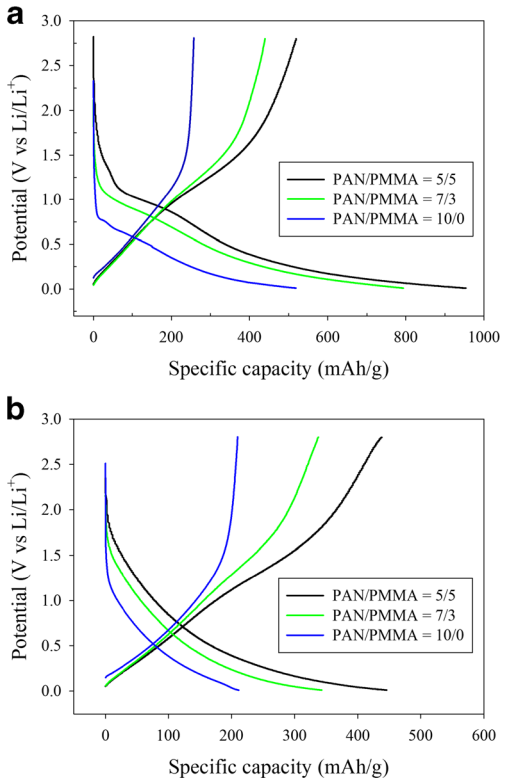

Fig. 6 Galvanostatic charge–discharge profiles of electrospun carbon nanofibers cycled at a current density of 150 mA/g. **a** 1st cycle and **b** 10th cycle

446 mAh/g for 7:3 PAN/PMMA- and 5:5 PAN/PMMA-derived carbon nanofibers, respectively. The 5:5 PAN/PMMA-prepared fibers exhibited a specific capacity greater than the theoretical value of graphite. When graphite is used as an anode material, lithium is only intercalated between graphitic layers, forming LiC_6. By contrast, when the low-crystalline carbon materials are used as an anode material, lithium is not only intercalated between graphitic layers but also located at the edge of the graphitic layer and on the surface of the crystallite. The three kinds of interaction between carbon and lithium allow the low-crystalline carbon materials to store more lithium than graphite [45, 46]. Additionally, the carbon materials thermally treated at low temperatures exhibit internal porosity and heteroatoms, which can also contribute to the specific capacity [47]. Therefore, the electrospun fibers can possess a specific capacity higher than graphite.

Figure 7 shows the rate capability of PAN- and PAN/PMMA-derived carbon nanofibers at current densities of 150, 300, 600, and 900 mA/g. For these measurements, we repeated 10 cycles for each current density. After 10 cycles for all the current densities, the specific capacity reached nearly a constant value, indicating that the carbon nanofibers were stable at those current densities. Table 2 lists the specific capacity of the carbon nanofibers obtained at various current densities. The specific capacity of the carbon nanofibers

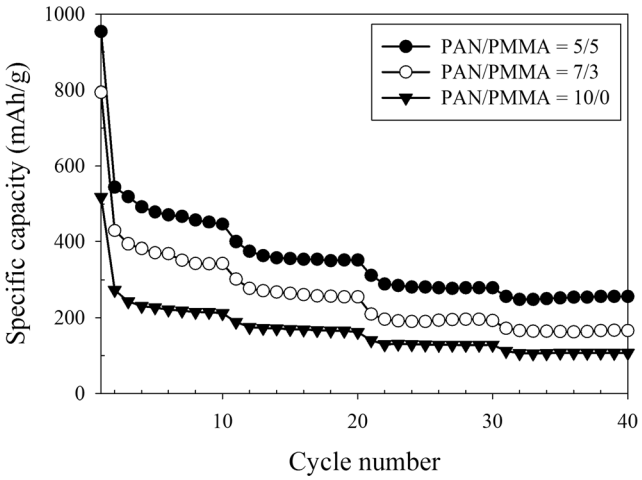

Fig. 7 Rate capacity of electron carbon nanofibers operated at different current densities

decreased with an increase in the current density. Once again, the PAN/PMMA-derived carbon nanofibers exhibited a greater specific capacity at each current density than the neat PAN-derived carbon nanofibers did. The addition of a higher amount of PMMA could further increase the specific capacity. The enhanced specific capacity of the PAN/PMMA-derived carbon nanofibers is attributed to the great number of mesopores and the high-specific surface area as well as the porous structure inside the fibers. These structures increased the active area of the carbon nanofibers and provided favorable contact with the electrolyte. Table 2 also shows the similar capacity retention for the various carbon nanofibers at each current density. The similar capacity retention of all the samples at each current density is attributed to the characteristics of the carbon nanofibers, providing favorable electron pathways and mechanical properties when used as an anode for lithium ion batteries.

Cycle life performance testing of the electrospun carbon nanofibers was conducted between 0.01–2.80 V at room temperature and the results are shown in Fig. 8. In the test, the cells were initiated at a current density of 100 mA/g for the first cycle, and then at a constant current density of 200 mA/g for a total of 100 cycles. For the electrospun carbon nanofibers, the

Table 2 The rate capacity of electrospun carbon nanofibers at various current densities

Sample	PAN/PMMA 10:0		PAN/PMMA 7:3		PAN/PMMA 5:5	
Current density (mA/g)	Specific capacity (mAh/g)	Capacity retention (%)	Specific capacity (mAh/g)	Capacity retention (%)	Specific capacity (mAh/g)	Capacity retention (%)
150	211	100	343	100	446	100
300	162	77	255	74	352	80
600	128	61	192	56	279	62
900	107	51	166	48	256	53

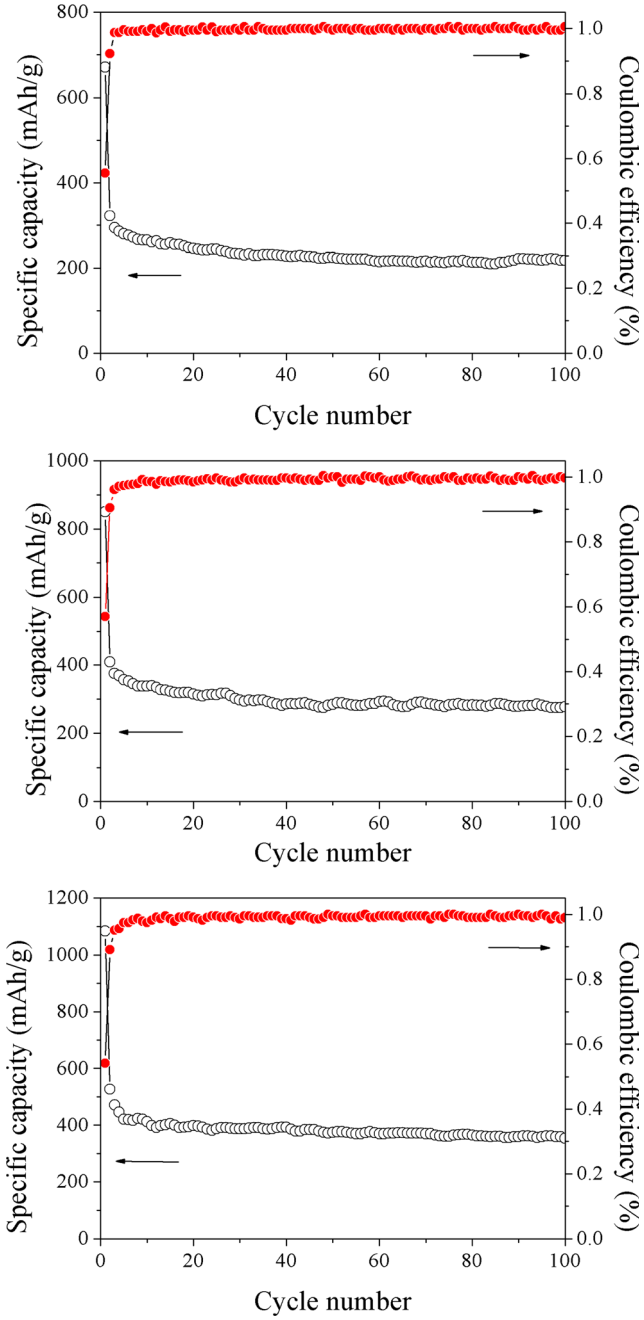

Fig. 8 Cycling performance of electron carbon nanofibers at a current density of 200 mA/g. **a** PAN/PMMA=10:0; **b** PAN/PMMA=7:3; and **c** PAN/PMMA=5:5

discharge capacity of the first cycle was 700–900 mAh/g, but the discharge capacity of the second cycle was reduced to 300–470 mAh/g. This was caused by both the formation of the SEI layer and the increased current density. After the second cycle, the discharge capacity decreased slightly and reached a near constant value at the end of the test. The steady cycle life performance suggested that the web morphology of the carbon nanofibers increased the stability of the fiber films. Figure 8 also shows the Coulombic efficiency, which is defined as the discharge capacity divided by the charge capacity of the same cycle. Because of the irreversible capacity caused by the formation of the SEI layer, the Coulombic efficiency of the first cycle was lower than 60 % for all samples. For the following cycles, the Columbic efficiency increased to almost 100 %, indicating that the electrospun carbon nanofibers were highly reversible during the charge and discharge processes. At the end of the test, the neat PAN-, 7:3 PAN/PMMA-, and 5:5 PAN/PMMA-derived carbon nanofibers exhibited discharge capacities of 218, 278, and 354 mAh/g, which corresponds to 67, 66, and 67 % retention in relation to the second discharge capacity. Our results suggest that the porous carbon nanofibers prepared by adding PMMA in a precursor solution improved the discharge capacity. Additionally, the web morphology provided favorable stability. The combination of these effects allows the porous carbon nanofibers to serve as a promising anode material for lithium ion batteries. The porous carbon nanofibers have applications not only in lithium ion batteries but also in supercapacitors, fuel cells, gas adsorption, and the removal of heavy metal ions [30, 48, 49].

Conclusion

In this study, we fabricated porous carbon nanofibers by electrospinning in a solution composed of PAN and PMMA to create lithium ion battery anode material. Because of the immiscibility of PAN and PMMA, they phase separated during electrospinning. Subsequent thermal treatment caused PAN carbonization and PMMA elimination, resulting in the formation of porous carbon nanofibers. The fiber diameter decreased with added PMMA content in the precursor solution. The addition of PMMA also facilitated the development of mesopores and micropores. The increased number of pores and decreased fiber diameter resulted in an increase in the specific surface area.

Electrochemical measurements on the electrospun carbon nanofibers revealed that the PAN/PMMA-derived carbon nanofibers exhibited a higher discharge specific capacity than the neat PAN-derived carbon nanofibers did for all tested current densities. The superior electrochemical performance of the PAN/PMMA-derived carbon nanofibers was attributed to the dominant mesopore volume and the high-specific surface area, which provided favorable contact between the fibers and electrolyte and facilitated the diffusion of electrolyte ions into the material. The 5:5 PAN/PMMA-derived carbon nanofibers exhibited a discharge capacity of 446 mAh/g at a current density of 150 mA/g. They exhibited a discharge capacity of 354 mAh/g after 100 cycles at a current density of 200 mA/g corresponding to 67 % retention, demonstrating the favorable cycle stability.

Acknowledgments This work is financially supported by the Ministry of Science and Technology in Taiwan under Grant No. 102-2221-E-006-018-MY3 and the Technology Development Program for Academia No. 103-EC-17-A-08-S1-204 by Ministry of Economic Affairs in Taiwan.

References

1. Jana M, Sil A, Ray S (2014) Morphology of carbon nanostructures and their electrochemical performance for lithium ion battery. J Phys Chem Solids 75:60–67
2. Liu XM, Huang ZD, Oh SW, Zhang B, Ma PC, Yuen M, Kim JK (2012) Carbon nanotube (CNT)-based composites as electrode material for rechargeable Li-ion batteries: a review. Compos Sci Technol 72:121–144
3. Yoo EJ, Kim J, Hosono E, Zhou HS, Kudo T, Honma I (2008) Large reversible Li storage of graphene nanosheet families for use in rechargeable lithium ion batteries. Nano Lett 8:2277–2282
4. Sun Y, Wu Q, Shi G (2011) Graphene based new energy materials. Energ Environ Sci 4:1113–1132
5. Wang G, Shen X, Yao J, Park J (2009) Graphene nanosheets for enhanced lithium storage in lithium ion batteries. Carbon 47:2049–2053
6. Kim C, Yang KS, Kojima M, Yoshida K, Kim YJ, Kim YA, Endo M (2006) Fabrication of electrospinning-derived carbon nanofiber webs for the anode material of lithium-ion secondary batteries. Adv Funct Mater 16:2393–2397
7. Ji L, Zhang X (2009) Fabrication of porous carbon nanofibers and their application as anode materials for rechargeable lithium-ion batteries. Nanotechnology 20:155705
8. Khan WS, Asmatulu R, Rodriguez V, Ceylan M (2014) Enhancing thermal and ionic conductivities of electrospun PAN and PMMA nanofibers by graphene nanoflake additions for battery-separator applications. Int J Energy Res 38:2044–2051
9. Peng YT, Lo CT (2015) Effect of microstructure and morphology of electrospun ultra-small carbon nanofibers on anode performances for lithium ion batteries. J Electrochem Soc 162:A1085–A1093
10. Endo M, Kim YA, Hayashi T, Nishimura K, Matusita T, Miyashita K, Dresselhaus MS (2001) Vapor-grown carbon fibers (VGCFs)—basic properties and their battery applications. Carbon 39:1287–1297
11. Zhang L, Aboagye A, Kelkar A, Lai C, Fong H (2014) A review: carbon nanofibers from electrospun polyacrylonitrile and their applications. J Mater Sci 49:463–480
12. Arshad SN, Naraghi M, Chasiotis I (2011) Strong carbon nanofibers from electrospun polyacrylonitrile. Carbon 49:1710–1719
13. Khan WS, Asmatulu R, Ceylan M, Jabbarnia A (2013) Recent progress on conventional and non-conventional electrospinning processes. Fiber Polym 14:1235–1247
14. Nuraje N, Khan WS, Lei Y, Ceylan M, Asmatulu R (2013) Superhydrophobic electrospun nanofibers. J Mater Chem 1:1929–1946
15. Ji L, Zhang X (2009) Generation of activated carbon nanofibers from electrospun polyacrylonitrile-zinc chloride composites for use as anodes in lithium-ion batteries. Electrochem Commun 11:684–687
16. Lee BS, Son SB, Park KM, Yu WR, Oh KH, Lee SH (2012) Anodic properties of hollow carbon nanofibers for Li-ion battery. J Power Sources 199:53–60
17. Wang L, Yu Y, Chen PC, Chen CH (2008) Electrospun carbon-cobalt composite nanofiber as an anode material for lithium ion batteries. Scr Mater 58:405–408
18. Yu Y, Gu L, Zhu C, Aken PA, Maier J (2009) Tin nanoparticles encapsulated in porous multichannel carbon microtubes: preparation by single-nozzle electrospinning and application as anode material for high-performance Li-based batteries. J Am Chem Soc 131:15984–15985
19. Ji L, Lin Z, Medford AJ, Zhang X (2009) In-situ encapsulation of nickel particles in electrospun carbon nanofibers and the resultant electrochemical performance. Chem Eur J 15:10718–10722
20. Ji L, Jung KH, Medford AJ, Zhang X (2009) Electrospun polyacrylonitrile fibers with dispersed Si nanoparticles and their electrochemical behaviors after carbonization. J Mater Chem 19:4992–4997
21. Choi HS, Lee JG, Lee HY, Kim SW, Park CR (2010) Effects of surrounding confinements of Si nanoparticles on Si-based anode performance for lithium ion batteries. Electrochim Acta 56:790–796
22. Hwang TH, Lee YM, Kong BS, Seo JS, Choi JW (2012) Electrospun core-shell fibers for robust silicon nanoparticle-based lithium ion battery anodes. Nano Lett 12:802–807
23. Wu Y, Balakrishna R, Reddy MV, Nair AS, Chowdari BVR, Ramakrishna S (2012) Functional properties of electrospun NiO/RuO_2 composite carbon nanofibers. J Alloy Compd 517:69–74
24. Chaudhari S, Srinivasan M (2012) 1D hollow alpha-Fe_2O_3 electrospun nanofibers as high performance anode material for lithium ion batteries. J Mater Chem 22:23049–23056
25. Kong J, Yee WA, Wei Y, Yang L, Ang JM, Phua SL, Wong SY, Zhou R, Dong Y, Li X, Lu X (2013) Silicon nanoparticles encapsulated in hollow graphitized carbon nanofibers for lithium ion battery anodes. Nanoscale 5:2967–2973
26. Ryu JH, Kim JW, Sung YE, Oh SM (2004) Failure modes of silicon powder negative electrode in lithium secondary batteries. Electrochem Solid-State Lett 7:A306–A309
27. Kasavajjula U, Wang CS, Appleby AJ (2007) Nano- and bulk-silicon-based insertion anodes for lithium-ion secondary cells. J Power Sources 163:1003–1039
28. Ji LW, Medford AJ, Zhang XW (2009) Electrospun polyacrylonitrile/zinc chloride composite nanofibers and their response to hydrogen sulfide. Polymer 50:605–612
29. Rahaman MSA, Ismail AF, Mustafa A (2007) A review of heat treatment on polyacrylonitrile fiber. Polym Degrad Stab 92:1421–1432
30. Niu H, Zhang J, Xie Z, Wang X, Lin T (2011) Preparation, structure and supercapacitance of bonded carbon nanofiber electrode materials. Carbon 49:2380–2388
31. Hsu YH, Lai CC, Ho CL, Lo CT (2014) Preparation of interconnected carbon nanofibers as electrodes for supercapacitors. Electrochim Acta 127:369–376
32. Hong CK, Yang KS, Oh SH, Ahn JH, Cho BH, Nah C (2008) Effect of blend composition on the morphology development of electrospun fibers based on PAN/PMMA blends. Polym Int 57:1357–1362
33. Goel SK, Beckman EJ (1994) Generation of microcellular polymeric foams using supercritical carbon-dioxide. 1. Effect of pressure and temperature on nucleation. Polym Eng Sci 34:1137–1147
34. Sutasinpromprae J, Jitjaicham S, Nithitanakul M, Meechaisue C, Supaphol P (2006) Preparation and characterization of ultrafine electrospun polyacrylonitrile fibers and their subsequent pyrolysis to carbon fibers. Polym Int 55:825–833
35. Xia K, Gao Q, Jiang J, Hu J (2008) Hierarchical porous carbons with controlled micropores and mesopores for supercapacitor electrode materials. Carbon 46:1718–1726
36. Fuertes AB, Lota G, Centeno TA, Frackowiak E (2005) Templated mesoporous carbons for supercapacitor application. Electrochim Acta 50:2799–2805
37. Lee GJ, Pyun SI (2006) Effect of microcrystallite structures on electrochemical characteristics of mesoporous carbon electrodes for electric double-layer capacitors. Electrochim Acta 51:3029–3038

38. Azaroff LV (1968) Elements of X-ray crystallography. McGraw-Hill, New York
39. Oya A, Marsh H (1982) Phenomena of catalytic graphitization. J Mater Sci 17:309–322
40. Dresselhaus MS, Dresselhaus G, Pimenta MA, Eklund PC (1999) In: Pelletier MJ (ed) Analytical application of Raman spectroscopy. Blackwell, London
41. Wang C, Appleby AJ, Little FE (2002) Irreversible capacities of graphite anode for lithium-ion batteries. J Electroanal Chem 519:9–17
42. Kumar PS, Sahay R, Aravindan V, Sundaramurthy J, Ling WC, Thavasi V, Mhaisalkar SG, Madhavi S, Ramakrishna S (2012) Free-standing electrospun carbon nanofibres—a high performance anode material for lithium-ion batteries. J Phys D: Appl Phys 45: 265302
43. Subramanian V, Zhu H, Wei B (2006) High rate reversibility anode materials of lithium batteries from vapor-grown carbon nanofibers. J Phys Chem B 110:7178–7183
44. Kim JS, Park YT (2000) Characteristics of surface films formed at a mesocarbon microbead electrode in a Li-ion battery. J Power Sources 91:172–176
45. Matsumura Y, Wang S, Kasuh T, Maeda T (1995) The dependence of reversible capacity of lithium ion rechargeable batteries on the crystal structure of carbon electrodes. Synth Met 71: 1755–1756
46. Wang S, Matsumura Y, Maeda T (1995) A model of the interaction between disordered carbon and lithium. Synth Met 71: 1759–1760
47. Flandrois S, Simon B (1999) Carbon materials for lithium-ion rechargeable batteries. Carbon 37:165–180
48. Kaneko K, Imai J (1989) Adsorption of NO_2 on activated carbon fibers. Carbon 27:954–955
49. Kang KC, Kin SS, Choi JW, Kwon SH (2008) Sorption of Cu^{2+} and Cd^{2+} onto acid- and base-pretreated granular activated carbon and activated carbon fiber samples. J Ind Eng Chem 14: 131–135